sciendo

Slovak Journal of Civil Engineering

Vol. 26, 2018, No. 4, 11 – 19

DOI: 10.2478/sjce-2018-0023

REGRESSION ANALYSIS OF SMALL STRAIN SHEAR AND CONSTRAINED MODULUS MEASUREMENTS ON SANDS WITH FINES: EFFECT OF DIFFERENT VOID RATIO FUNCTIONS USED

Jakub PANUŠKA[1]*, Jana FRANKOVSKÁ[1]

Abstract

The article is focused on a regression analysis of small strain shear and constrained modulus measurements of 15 different natural sands with plastic fines from the Pannonian basin. Measurements done within this work are supported by additional data on sands with plastic and non-plastic fines gathered from the literature in order to demonstrate the versatility of the approaches used and behavior observed. Bender / extender element techniques are used in this study for measuring the small strain shear and constrained modulus of sands with fines. Three void ratio functions, which are commonly used in predictive empirical equations for predicting small strain stiffness, with corresponding fitted parameters are presented, and their effect on the accuracy of the regression procedure is studied. It is assumed that all the void ratio functions tested provide nearly the same degree of accuracy and that the fitted models are able to predict the values of the parameters measured within an acceptable range of errors. Finally, proposed constant regression constants for sands with plastic fines are given.

Address

[1] Dept. of Geotechnics, Faculty of Civil Engineering, Slovak University of Technology, Bratislava, Slovakia

* ***Corresponding author:*** jakub.panuska@stuba.sk

Key words

- Small strain stiffness,
- Accuracy of empirical prediction,
- Effect of void ratio function,
- Regression analysis,
- Plastic fines.

1 INTRODUCTION

1.1 Importance of small strain stiffness

Despite the nonlinear nature of soil behavior in general, the importance of soil stiffness in the range of small and very small shear strains ($\gamma = 10^{-6} – 10^{-5}$) has recently attracted increasing interest. Conventional laboratory tests (i.e., oedometer tests, triaxial tests) measure stiffness only in a range of intermediate to large strains (Atkinson & Sallfors, 1991). Such strains occur solely in the vicinity of structures (i.e., foundations, tunnels, retaining structures) when loaded. Thus, the stiffness of soil is grossly underestimated outside zones of large strains. Although engineers usually consider increases in stiffness with depths, the dependence of stiffness on imposed strain levels is somewhat overlooked. Strain - dependent stiffness models are quite widely recognized (Oztoprak & Bolton, 2013), (Hardin & Drnevich, 1972), (Ishibashi & Zhang, 1993). These models are able to predict the degradation of stiffness relatively well with acceptable differences, while the prediction of small strain stiffness (one of the basic inputs to strain - dependent stiffness models) is still quite challenging and studied intensively (Hardin & Richart, 1963), (Iwasaki & Tatsuoka, 1977), (Payan, et al., 2016a), (Senetakis, et al., 2012), (Wichtmann, et al., 2015). As natural soils are quite complex materials, there has recently been an increased effort to describe the behavior of mixtures of coarse and fine - grained soils. While the small strain stiffness of mixtures of sands with non-plastic fines are captured quite well (Goudrazy, et al., 2016), (Salgado, et al., 2000), (Wichtmann, et al., 2015), (Yang & Liu, 2016), the effect of plastic fines has not been studied so intensively, though significant differences between these two types of fines have been found (Carraro, et al., 2009).

1.2 Empirical formulation of small strain shear and constrained modulus

A well - recognized and widely used empirical relationship for the small strain shear modulus, G_{max}, of sand can be written as (p', patm and G_{max} in kPa) (Hardin & Richart, 1963):

$$G_{max}=A.F(e).\left(\frac{p'}{p_{atm}}\right)^{n}.p_{atm} \quad (1)$$

where A is a material constant; $F(e)$ is a void ratio function; n is a stress exponent accounting for the dependency of G_{max} on the mean effective stress p'; and p_{atm} is the normalizing pressure usually assumed to be atmospheric pressure, i.e., 100 kPa. The same form of equation *(1)* was used for a prediction of a small strain constrained modulus M_{max} in (Wichtmann & Triantafyllidis, 2010), (Senetakis, et al., 2017):

$$M_{max}=A.F(e).\left(\frac{p'}{p_{atm}}\right)^{n}.p_{atm} \quad (2)$$

where the meaning of the parameters remains the same as in equation *(1)*. The void ratio function $F(e)$ is an important parameter as it captures the dependency of both M_{max} and G_{max} on the void ratio, i.e., as the void ratio decreases, the small strain stiffness increases and vice versa. Three types of void ratio functions are studied here, i.e:
the void ratio function proposed by Hardin and Richart (Hardin & Richart, 1963),

$$F(e)_H=\frac{(a_H-e)^2}{1+e} \quad (3)$$

the void ratio function proposed by Jamiolkowski et al. (Jamiolkowski, et al., 1991),

$$F(e)_J=e^{-a_J} \quad (4)$$

And the void ratio function proposed by Shibuya et al. (Shibuya, et al., 1997).

$$F(e)_S=(1+e)^{-a_S} \quad (5)$$

The parameters a_H, a_J and a_S (i.e., in general a) are variables of equations *(3), (4)* and *(5)*. Parameters A, n and a are obtained through best fit regression analysis (usually the least squares method) of equations *(1)* and *(2)* for the experimentally measured results. Note that a_H, a_J and a_S may vary for each type of sample or may be assumed as constants for some typical range of materials (i.e., for sand, clay, etc.). Applications of different void ratio functions in various studies are presented in Tab. 1. Note that commonly used coefficients for various soils have been posted by the authors of equations (*3 – 5*) as $a_H = 2.17$; $a_J = 1.3$; $a_S = 2.4$ or $a_S = 3.0$ in (Oztoprak & Bolton, 2013).

1.3 Aim of the study

The proposed article studies the effect of different void ratio functions, defined by equations *(3), (4)* and *(5)* on the predictive accuracy of the results of the small strain shear and the constrained modulus measured for sand with plastic fines for samples as predicted by empirical equations *(1)* and *(2)* (note that the predictions and measurements are going to be compared in a normalized form, i.e., the shear and constrained modulus normalized by the void ratio function). The analysis is focused on cases with void ratio functions with a variable parameter a (i.e., a varies in order to find the least squared residual error) and cases with parameter a estimated as mean (or the best fit with the lowest squared error for M_{max}) of all the regressed values, while the values outside the ± 1 x standard deviation are not considered in the estimation of the mean. Data gathered from the literature for sand with plastic and non-plastic fines are used to support the measurements from this study and complete the whole picture of this problem.

2 MATERIALS AND METHODS

2.1 Material tested, preparation of samples, and testing procedure

The material tested consist of 15 different natural sands, while one sand was tested with and without gravely particles (the gravel

Tab. 1 *Void ratio functions and stress exponents according to various authors (modified after (Benz, 2007)). * - sand with non-plastic fines; ** - sand with plastic fines*

Soil	$F(e)$ (-)	n (-)	Reference
Toyoura sand (subangular)	$e^{-1.3}$	0.45	(Lo Presti, et al., 1993)
Normally consolidated clay	$(1+e)^{-2.4}$	0.5	(Shibuya, et al., 1997)
Ticino sand (subangular)	$(2.27-e)^2/(1+e)$	0.43	(Lo Presti, et al., 1993)
Ottawa sand No. 20-30	$(2.17-e)^2/(1+e)$	0.5	(Hardin & Richart, 1963)
Quiou carbonated sand	$e^{-1.3}$	0.62	(Lo Presti, et al., 1993)
Various sands	$(1+e)^{-3}$	0.49-0.51	(Oztoprak & Bolton, 2013)
26 quartz sand	$(a_H-e)^2/(1+e)$ a_H = 1.08-2.34	0.41-0.58	(Wichtmann & Triantafyllidis, 2009)
13 quart sands with fines *	$(a_H-e)^2/(1+e)$ a_H = 0.62-6.55	0.44-0.66	(Wichtmann, et al., 2015)
Ottawa sand with fines *	$(2.17-e)^2/(1+e)$	0.44-0.81	(Salgado, et al., 2000)
Ottawa sand with fines *	e^{-a_J} $-a_J$ = 1.04-2.38	0.44-0.72	(Salgado, et al., 2000)
Ottawa sand with fines **	$(2.17-e)^2/(1+e)$	0.47-0.49	(Carraro, et al., 2009)
Toyoura sand *	$(2.17-e)^2/(1+e)$	0.37-0.40	(Yang & Liu, 2016)
Firoozkooh sand *;**	e^{-a_J} $-a_J$ = 1.05-4.17	0.36-0.51	(Paydar & Ahmadi, 2016)

Tab. 2 *Grain size properties and physical properties of the natural sands tested*

Sample	d_{60} (mm)	d_{50} (mm)	d_{30} (mm)	d_{10} (mm)	C_u (-)	FC (%)	e_{max} (-)	e_{min} (-)	ρ_S (g/cm^3)
P1	0.284	0.243	0.180	0.130	2.18	5.69	0.788	0.516	2.680
P2	0.459	0.424	0.311	0.193	2.38	1.32	0.699	0.468	2.659
P3	0.439	0.365	0.244	0.160	2.74	0.25	0.668	0.453	2.660
P4	0.207	0.179	0.121	0.010	20.70	16.75	0.854	0.480	2.678
P5	0.377	0.322	0.230	0.151	2.50	3.26	0.762	0.488	2.664
P6	0.225	0.211	0.172	0.109	2.06	7.56	0.790	0.494	2.674
P7	0.128	0.107	0.074	0.013	9.85	21.11	0.949	0.524	2.708
P8	0.149	0.129	0.091	0.022	6.77	20.20	1.241	0.702	2.722
B1	0.216	0.191	0.123	0.007	30.86	18.84	0.901	0.424	2.689
B1gr	0.233	0.211	0.136	0.011	21.18	16.48	0.716	0.380	2.689
B2	0.237	0.218	0.170	0.109	2.17	3.05	0.757	0.496	2.654
PS	0.488	0.435	0.287	0.177	2.76	1.14	0.596	0.426	2.642
S1	0.256	0.236	0.193	0.114	2.25	7.00	1.189	0.754	2.675
S2	0.404	0.329	0.210	0.028	14.43	12.91	0.967	0.563	2.662

was presented as 15 % of the overall mass). A testing matrix was created by 15 samples of natural sand with different contents of fines (only three sands contained around 1 % or less fines). All the natural sand tested comes from the geographical location of the Pannonian basin. The sand from Plavecký Štvrtok (PS) is an aeolic type of sand with round grains. A sample was taken directly from the surface near an open pit. The samples from the locality of Sandberg (S1, S2) are Neogene sands deposited on a former Neogene beach on the edge of a sea. Two sands were sampled from an exposed wall. The Győr (G), Budapest (B1, B1gr, B2), and Paks (P1 - P8) sands, according to (Szilvágyi, 2018), are typical Danubian sands formed by the river Danube and flooding in its vicinity. Thus, the sands are characterized as fluvial sands, but were also partially transported by wind when the sands were exposed to the atmosphere on the surface. The grain size and physical properties of the sands tested are shown in Tab. 2. The fines were characterized as particles with diameters < 0.063 mm. The grain size curves of the sands tested are shown in Fig. 1.

In Tab. 2, d_{10}, d_{30}, d_{50} and d_{60} represent particle diameters at *10*, *30*, *50* and *60* % of the particle percentages passing by weight; C_u is the uniformity coefficient; *FC* is the content of the fines; e_{min} and e_{max} are the minimum and maximum void ratios; ρ_S is the specific gravity of the particles; w_L is the liquid limit; w_P is the plasticity limit; and I_P is the plasticity index. Clean sand, i.e., the sand matrix if the fines are extracted, is characterized as sand with quite similar gradations. The uniformity of clean sand varies between the values of 1.68 – 2.76; thus sands with a similar uniformity were tested. The fines are characterized as low to medium plasticity clays or medium plasticity silts. The fines exhibit a similar I_P 10.25 – 18.46 %. Thus, we may characterize the fines as plastic. Note that all the fines of all the sands are characterized as plastic due to the same origin of the samples even if their plasticity was not tested. This idea is supported by measurements where all the samples follow the same trends. Note that the sands tested in this study have been completed by tests performed on sands with the plastic (Carraro, et al., 2009) and non-plastic (Salgado, et al., 2000), (Wichtmann, et al., 2015), (Yang & Liu, 2016) fines found in the literature. All of the measurements of G_{max} and M_{max} presented in (Wichtmann, et al., 2015) were provided by Prof. Wichtmann, whose contribution is acknowledged. The rest of the data were extracted with the aid of a WebPlotDigitizer tool (Rohatgi, 2017) from the original papers of the authors cited.

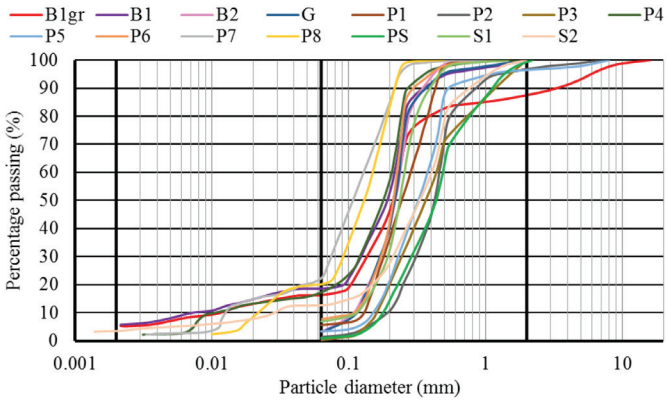

Fig. 1 *Grain size curves of the natural sands tested*

All the specimens tested in this study were prepared in a dry state under three different void ratios for each sand tested. The specimens have approximately a 50 mm diameter and 100 mm height. The three different void ratios were obtained by different procedures. For the highest void ratio, sand was only poured inside a latex membrane supported by a steel mold; for the medium void ratio, sand was filled inside the membrane in three layers. Three to five taps were applied to the side of the mold to densify the layer, and the lowest void ratio was achieved by filling the sand in three layers inside, tapping the side of the mold, and tamping the sand from the top. Subsequently, the top cap was put on, and the latex membrane was rolled over the cap with a sealing O – ring. After the preparation of the specimen, a vacuum of 50 kPa was applied to the specimen; thus $p' = 50$ kPa. The steel mold was dismantled as the confinement was applied and the cell attached. A load cell was then moved to gently touch the specimen. Then, the cell was filled with water, and the pressure of the water was increased gradually to 50 kPa, while the vacuum was continuously decreased to keep $p' = 50$ kPa. The confinement of 50 kPa was assumed as

the first stress level of the testing, and at least 7 stress levels were applied up to 400 kPa with steps of 50 kPa. Bender / extender tests were performed at each stress level. All the tests were performed in an isotropic state of stress, i.e., q = 0 kPa. This study generated 418 measurements of G_{max} and 416 measurements of M_{max} at the different void ratios and confinement levels.

Changes in the volume of the dry sands under such conditions were assumed according to an isotropic deformation, i.e., $3.\varepsilon_a = \varepsilon_v$ (Gu, et al., 2015); ε_a is the axial, and ε_v – is the volumetric strain. Thus only the axial deformation had to be measured. The load at the top cap was kept constant at a value of 0.01 kN (q = 5kPa); thus when the next level of confinement was applied, the lower chamber of the Bishop and Wesley triaxial system had to move up to maintain the load, and the LVDT measured the axial deformation.

2.2 Evaluation of the bender / extender elements tests

The point of interest of this study is the measurement of small strain shear G_{max} and constrained M_{max} modulus. These are estimated through the values of shear v_s and compressional v_p wave velocities propagating along a sample´s axis when the density ρ of the samples is known as:

$$G_{max}=v_s^2.\rho \tag{6}$$

$$M_{max}=v_p^2.\rho \tag{7}$$

The bender / extender elements (BEE) installed in the top cap and bottom pedestal of the Bishop and Wesley triaxial cell manufactured by GDS Instruments were used to measure the v_s and compressional v_p in the soil specimens. The bender / extender elements are plate piezoceramic elements. One of the first applications of piezo transducers in soil mechanics and geotechnical engineering was presented in (Shirley & Hampton, 1978). Later on (Schultheiss, 1981) measured the shear wave velocity v_s, and, in addition, the compression wave velocity v_p with two decoupled piezo transducers were used for the introduction of shear and compression waves into soil.

Shear and compression waves have to somehow be introduced into soil. Plate elements act as a cantilever beam which, when voltage is applied, can perform shear - like movements (i.e., move from side to side) or elongations (the movement depends on the polarization and wiring of the elements). It was quite common to use two decoupled elements for the production of P and S waves until Lings and Greening (Lings & Greening, 2001) came up with the idea of a coupled transducer, which could produce both S and P waves in a single pair of elements if a certain polarization and wiring of the elements was used; these principles are used in this study.

The evaluation of the measurement of the shear and compressional wave velocity is done by means of so - called travel time, i.e., tt_{vs} (shear wave) and tt_{vp} (compression wave). Travel time is the time needed to travel the distance between the two elements, i.e., a transmitter and a receiver. The distance between the two elements L_{BEE} is usually assumed to be a tip – to – tip distance between the elements (Yamashita, et al., 2009). If this distance is known, the shear or compressional wave velocity can be computed as:

$$v_s=\frac{L_{BEE}}{tt_{vs}} \; or \; v_p=\frac{L_{BEE}}{tt_{vp}} \tag{8}$$

The estimation of the travel time is the most important part of the testing and involves the highest level of uncertainties and errors, such as the near field effect (Sanchez-Salinero, et al., 1986), (Jovicic, et al., 1996), dispersion (waves with different frequencies travel with different phase velocities) (Greening & Nash, 2004), the reflection of the waves from the specimen and the testing system´s boundaries, and electromagnetical coupling between the elements – (the "cross - talk" effect) (Lee & Santamarina, 2005). Several waveforms and various frequencies may be triggered as inputs for shear and compression waves. Various waveforms used in the bender element tests have been well reviewed in (Viana Da Fonseca, et al., 2008). The frequencies, waveforms, and evaluation methods employed in this study are presented in Tab. 3.

Tab. 3 *Input signals and evaluation methods used in the BEE testing*

Input signal	Evaluation method	Frequency of signal
1 x sine wave	PtP (S-wave)/StS(P-wave)	1; 2; 3.3; 5; 10; 20 kHz
	CC	
4 x sine wave	PtP (S-wave)/StS(P-wave)	3.3; 5; 9; 17 kHz
	CC	
Sine sweep	PtP (S-wave)/StS(P-wave)	5 – 10 kHz 3 ms duration
	CC	5 – 25 kHz 2 ms duration
	FD	5 – 50 kHz 1 ms duration
		5 – 100 kHz 0.5 ms duration

Several methods of interpreting measurements, i.e., estimating the shear tt_{vs} and compression tt_{vp}, wave travel time can be used. The Start-to-Start (*StS*), Peak-to-Peak (*PtP*), Cross-Correlation (*CC*), and frequency domain (*FD*) approaches were used to estimate the corresponding travel time. *StS*, *PtP* and *CC* were applied to estimate tt_{vp} and *PtP*; *CC* and *FD* were applied to estimate tt_{vs}. These methods were incorporated in a MatLab (MathWorks Inc., 2017) code (Panuška, 2018). The peak-to-peak estimation of the shear wave´s travel time is based on the measurement of the time delay between the first peaks of the sent and received signals (Fig. 2). The first significant peak of the received signal was assumed to be a signal with a 30-50 % magnitude of the maximum amplitude measured on the output (see, e.g., (Yamashita, et al., 2009)). This rule of thumb is incorporated due to the probable occurrence of higher peaks at a later travel time, which is usually caused by the reflected waves. In general, the *CC* method of tt_{vs} may be seen as a better substitute for *StS,* as the *CC* usually indicates the start of the input signal waveform in a measured output waveform (Fig. 2). The resulting cross correlation coefficient reaches a maximum when the input and output signals match the best at a given position on the time axis. Note that once again the first significant peak of *CC* was assumed to be a peak with a 30-50 % magnitude of the maximum *CC* coefficient due to the reasons mentioned above. No other details about this broad topic will be introduced due to the lack of space, so the reader is referred to, e.g. (Yamashita, et al., 2009), (Ogino, et al., 2015). The frequency domain evaluation of tt_{vs} is based on the measurement of the group´s velocity delay in a frequency versus the unwrapped phase plot (Fig. 3), (Greening & Nash, 2004), (Viana Da Fonseca, et al., 2008). The unwrapped phase is obtained from the transfer function between the sent and received signals. Note that the measurement of the phase velocity delay is not performed here, but some sort of dispersion is present in the bender element measurement system; therefore, the phase and group velocities are slightly different (Greening & Nash, 2004). The moving window algorithm (Viana Da Fonseca, et al., 2008) was used to obtain the resultant tt_{vs} with a width of the frequency window of 1000 – 11000 Hz. The resulting tt_{vs} and thus v_s and G_{max}, were obtained by averaging

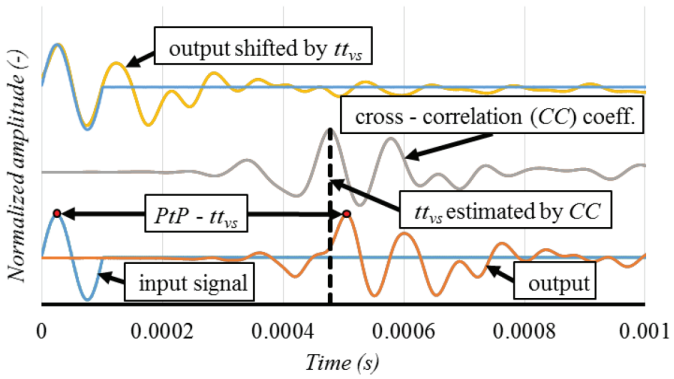

Fig. 2 *Estimation of tt_{vs} by the PtP and CC methods*

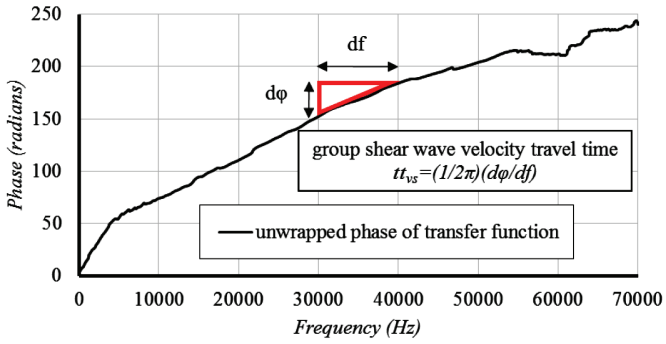

Fig. 3 *Estimation of tt_{vs} by the FD method*

the results of v_s within a range of ± 5 m/s. This range was found by inspecting the results of all three evaluation methods as the most probable interval of the correct shear wave´s arrival time. This procedure was verified by independent sets of measurements with the Resonant Column (RC) device (Szilvágyi, 2018), (Panuška, 2018). The values of G_{max} measured by *RC* and *BEE* fall within the range of a ±15 % difference, which was also found in the literature (e.g., Toyoura sand (Yamashita, et al., 2009)). The estimation of tt_{vp} by *PtP* (Senetakis, et al., 2017) and *CC* completely follows the ideas applied to tt_{vs}. Additionally, the *StS* method was employed to estimate tt_{vp} because it is easier to observe the first direct arrival of the P-wave with a comparison of the S-wave (no near field effects in P-wave measurements and minimization effect of influence of the reflected waves).

The first arrival (i.e., tt_{vp}) is assumed to be at the point of the first steep increase in an output signal (Wichtmann & Triantafyllidis, 2010), (Senetakis, et al., 2017). The procedure for averaging and obtaining the final values of v_p and M_{max} is the same as for v_s and G_{max}.

2.3 Normalization of the results and regression analysis employed

The normalization of the small strain stiffness with respect to the void ratio enables one to compare samples with different void ratios and observe the dependency of the small strain stiffness solely on the confinement level. On the other hand, normalization with respect to the confinement level enables one to observe the dependency of the small strain stiffness on the void ratio. A normalization procedure of this kind may be found, e.g., in (Gu, et al., 2013). The results from the three tests with different void ratios are depicted in Fig. 4. Normalization was done with respect to Eq. 1 with the void ratio function presented by Eq. 3 and a_H = 2.17. The equations in Fig. 4b and 4c represent Eq. 1 after some minor rearrangements. Figure 4b represents the shear modulus normalized by the void ratio function (note that all three different void ratios fall onto one line after normalization); the right side contains coefficients *A* and *n* from Eq. 1, i.e., the form of the equations represents general power equations. Parameters *A* and *n* are regressed through the least squares method in order to minimize the residual sum of the squares between the predicted and measured values to obtain the best fit. Additionally, Figure 4c represents the shear modulus normalized by confinement, and the equation in this figure is rearranged in this way. Thus, only parameters *A* and $F(e)_H$, in this case with a_H = 2.17, remain on the right side, and these will be regressed. Note that a_H (or *a* in general) may be set as a variable and may be regressed as well. It must be highlighted that these two plots are inter - related. Parameter *A* is presented in both plots on the right side; additionally, parameters *F(e)* (thus also *a*) and *n* are presented once in the regression procedure and the second time as a normalization factor. Due to this inter - relationship, it was decided to regress both forms of Eq. 1 presented in Fig. 4b

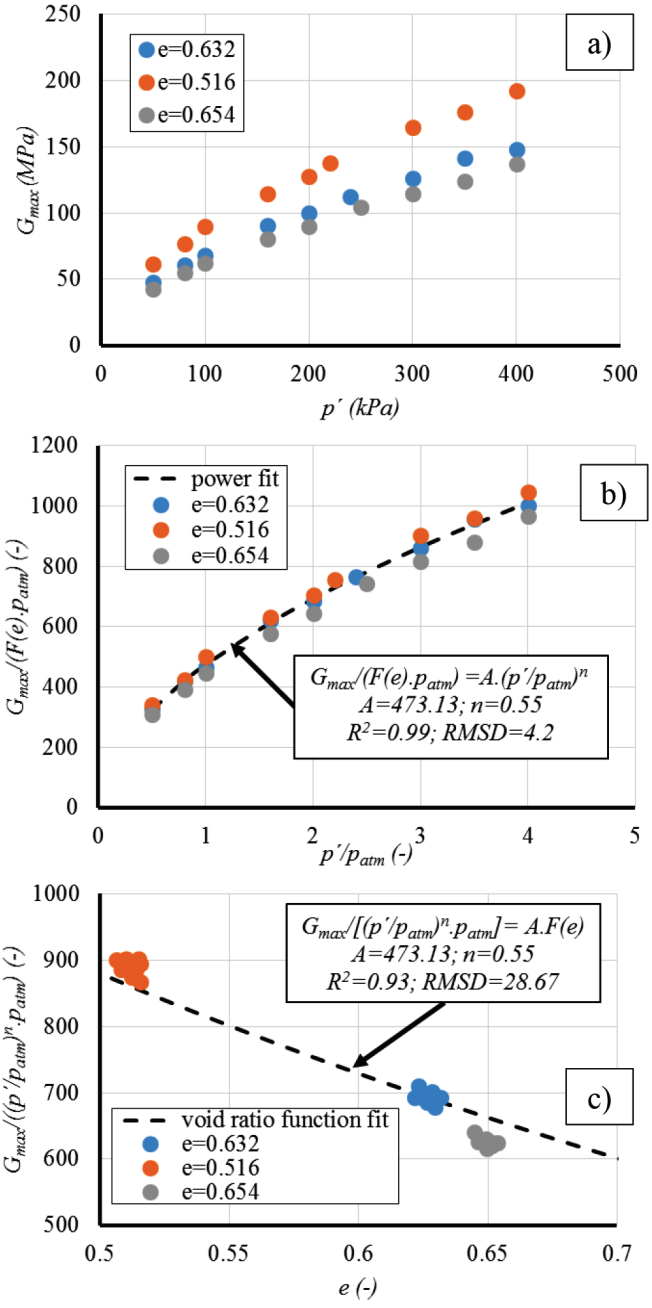

Fig. 4 *Measured G_{max} for sample P2 a) for the three void ratios; b) normalized by the void ratio function; c) normalized by confinement*

and 4c simultaneously, i.e., a summation of the residual squared errors was computed, and this was minimized rather than obtaining a single sum of the residual squared errors for each form separately. The modulus normalized by the void ratio function and by confinement may differ in magnitude; thus, they were scaled to be equal in magnitude. The scaling factor was calculated with respect to the modulus normalized by the void ratio. The Excel solver add-in was used for this multivariate optimization to find the minimum value of the sum of the squared residuals. The coefficient of determination R^2 was estimated for each single regression analysis; however, this parameter only evaluates the goodness of fit qualitatively. Thus the Root-Mean-Square-Deviation (*RMSD*) is used as a quantitative measure of accuracy as this parameter represents the standard deviation of the prediction with respect to measurement. The *RMSD* was used for a similar purpose, e.g., in (Goudrazy, et al., 2016) and is defined as:

$$RMSD=\sqrt{\frac{\sum_{i=1}^{N}(y_{mi}-y_{pi})^2}{N}} \quad (9)$$

where y_{mi} is the measured value; y_{pi} is the predicted value; and N is the number of samples.

3 RESULTS AND DISCUSSION

The first analysis was performed with the void ratio function´s parameter a included in the regression procedure in order to obtain a set of best fit parameters for the single samples. The predictive model based on the correlation of A, n and a on the grainsize properties of sands with fines was developed in (Panuška, 2018). Such a model is not discussed here as it is beyond the scope of this article. The results of the regression for the fitted parameter a are plotted in Fig. 5. Note that the mean grain size was chosen to be plotted on a horizontal axis in order to distinguish the different samples. The mean grain size was also chosen because it is a parameter which has been said to have no influence on G_{max} (Iwasaki & Tatsuoka, 1977) (Wichtmann & Triantafyllidis, 2009), and M_{max} (Wichtmann & Triantafyllidis, 2010). There are no doubts about this fact as it was extensively experimentally observed. However d_{50} may influence some parameters of Eq. 1 or parameters of the different void ratio functions rather than the small strain stiffness itself. This fact can be observed in Fig. 5, where, for both G_{max} and M_{max}, the significant dependency of a_H (used in Eq. 3) on d_{50} is found, while such behavior seems to be lost if Eqs. 4 or 5 are used in the regression. Additionally, Fig. 5 revealed that the commonly used void ratio function parameters $a_H = 2.17$ (Hardin & Richart, 1963) and $a_J = 1.3$ (Jamiolkowski, et al., 1991) were found to represent the mean of the regressed values (a_H does not, but is very close to the mean; however, it gave the best results in the predictive model) for sands with fines in the case of G_{max}, while the value of $a_S = 3.57$ is higher than presented in (Shibuya, et al., 1997) or (Oztoprak & Bolton, 2013). Subsequently, the value of $a_H = 2.17$ seems to fit well for the regressed data; in addition, it gives the best prediction of the measured values for M_{max} measurements. The value of parameter $a_J =$

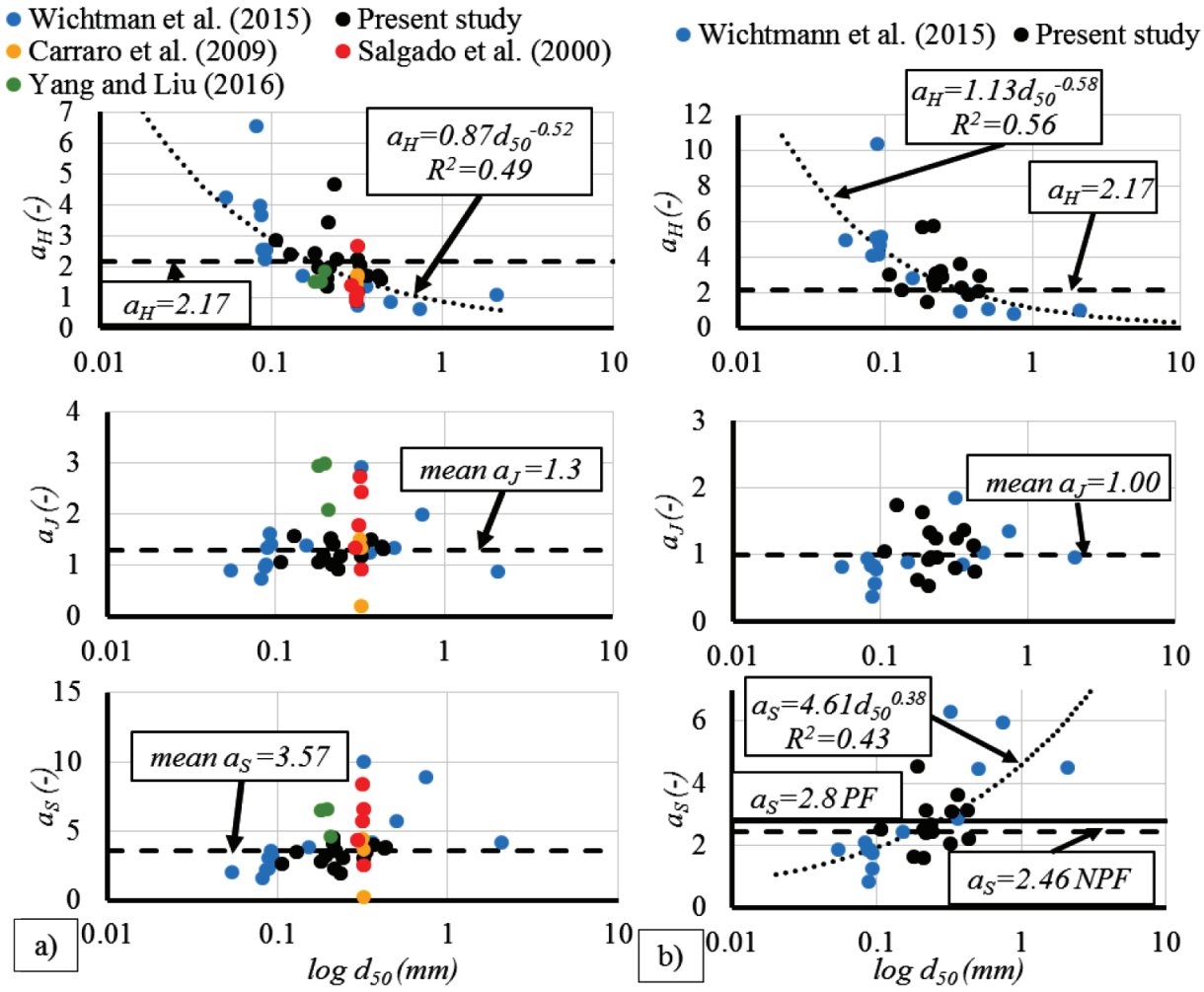

Fig. 5 *Regressed and mean/best fit values of a_H; a_J and a_S for the different void ratios functions a) for G_{max}; b) for M_{max}*

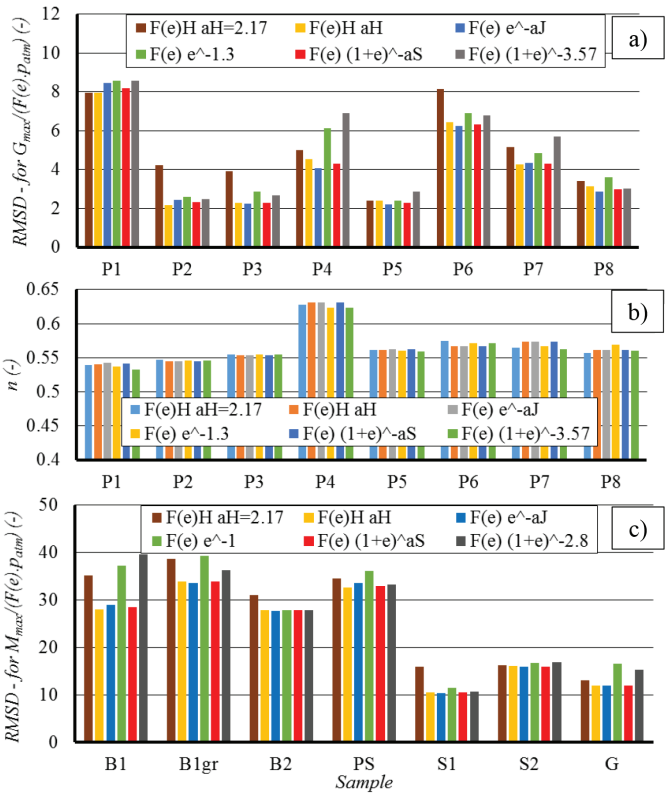

Fig. 6 *Results of regression analysis for different void ratio functions employed: a) RMSD for the void ratio normalized G_{max}; b) variation of the stress exponent n; c) RMSD for the void ratio normalized M_{max}*

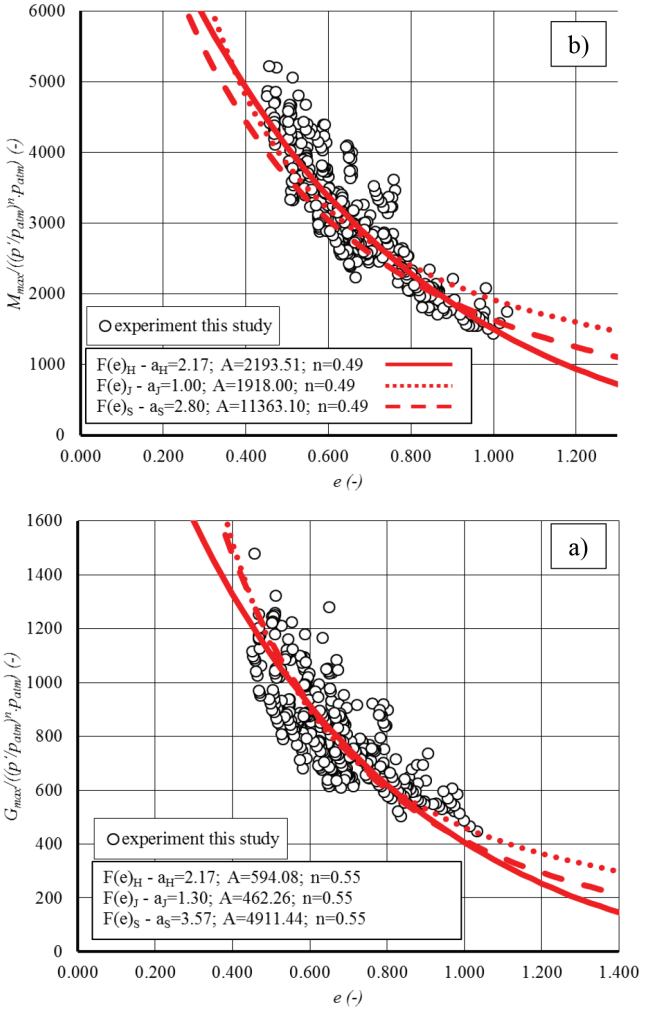

Fig. 7 *Prediction of the confinement normalized modulus based on the different void ratio functions a) confinement normalized small strain shear stiffness G_{max}; b) confinement normalized small strain constrained stiffness M_{max}*

1.0 and a_S = 2.8 (for plastic fines – PF) and a_S = 2.46 (for non-plastic fines – NPF), have been found to represent the average value of the void ratio function´s parameter *a* for sands with fines in the case of M_{max} measurements. According to the regression analysis performed, parameter *a* was selected regardless of the plasticity of the fines, with the exception of void ratio function Eq. 5 for the measurement of M_{max}. Such a simplification produces only a minor difference in the constant value of parameter *a*. Note that the values of a_S were found by minimizing the errors of the predictive model but are very close to the mean of the regressed data.

The constant values of *a* discussed above were used in the second round of the regression where only the parameters *A* and *n* were regressed in order to minimize the sum of the squared errors of the normalized modulus. A comparison of *RMSD* for the void ratio´s normalized modulus in the case of the constant and regressed *a* employed is presented in Fig. 6a. Despite the higher value of *RMSD* in the case of the constant *a* employed, the resulting degree of accuracy did not suffer a significant loss as the maximum *RMSD* difference for the constant and regressed void ratio parameter *a* is up to 3 for sample P4 if Eq. 5 is used. Note that only half of the samples are shown due to the lack of space and that the second group only showed small differences. The second group of samples were used for a comparison for M_{max}, and a similar trend can be observed. However, the *RMSD* is around 4 – 5 times higher, but the M_{max} in general is 4 times higher than G_{max}; thus the relative error remained approximately the same. The greatest difference in *RMSD* (up to 10) may be found for sample B1 if Eq. 5 is used. Additionally, according to Fig. 6b, the stress exponent *n* is independent of the different void ratio functions used in the regression

Tab. 4 *Proposed constant regression coefficients and error estimates for the samples tested in this study*

Empirical equation and void ratio function employed		Regression coefficients			Percentage of samples in error range		
		A	a	n	± 10 %	± 20 %	± 30 %
Eq. 1	Eq. 3	594.08	2.17	0.55	42.11 %	80.86 %	95.93 %
	Eq. 4	462.26	1.30		46.17 %	79.67 %	97.37 %
	Eq. 5	4911.44	3.57		41.15 %	76.56 %	95.45 %
Eq. 2	Eq. 3	2193.51	2.17	0.49	62.02 %	89.18 %	99.52 %
	Eq. 4	1918.00	1.00		56.49 %	87.26 %	99.76 %
	Eq. 5	11363.10	2.80		53.61 %	86.30 %	97.60 %

and is also independent of the void ratio function parameter *a*, i.e., if it is regressed or set constant. The proposed regression coefficients for Eqs. 1 and 2 are shown in Tab. 4. Note that while parameter *a* is based on the regression of the entire dataset, including data from the literature, parameters *A* and *n* are based on the average of the values regressed only for the single sand tested in this study. Thus the regression coefficients proposed in Tab. 4 are applicable only for sands with plastic fines. The error among the different approaches is less than 5 % for G_{max} and 10 % for $M_{max.}$

The prediction of the small strain shear and constrained modulus normalized by confinement is presented in Fig. 7. Fig. 7a shows that all the predictions based on the different void ratio functions overlap each other in the void ratio range of the specimens tested in this study, i.e., 0.4 – 1.0. However, they start to deviate outside of this range. Similar findings are shown in Fig. 7b with only slight deviations among the different void ratio functions employed. In general, the parameters proposed in Tab. 4 resulted in good predictions for the small strain shear and constrained modulus of the sands with plastic fines measured in this study.

4 CONCLUSIONS

This study analyzed the effect of different void ratio functions on the accuracy of the empirical equations used for predicting the small strain shear and constrained modulus. The void ratio function parameter *a* was set for each void ratio function as a constant value based on the mean of the regressed values for sands with plastic and non-plastic fines from this study and gathered from the literature. The regression analysis has shown that there is a very small or negligible influence on predictions of small strain stiffness, whether the void ratio parameter *a* (a_H, a_J, a_S) is included in the regression or set constant as proposed in this study. Additionally, the different void ratio functions employed in the regression procedure produced only minor deviations among their predictions of the measured G_{max} and M_{max} in this study. Two void ratio function parameters were found to fit the proposals of the original authors very well, i.e., a_H = 2.17; a_J = 1.30 in the case of G_{max} measurements. The rest of the parameters obtained through the regression analysis performed in this study are shown in Tab. 4. This table also includes newly - proposed parameters *A* and *n*, for predicting the M_{max} of sands with plastic fines. The values of *a* were set independently of the plasticity of the fines, as this produces only minor differences. However, parameters *A* and *n* were set as a mean of the single regressed values only for the sands tested in this study. Thus, the proposed values are recommended only for predicting the small strain stiffness of normally consolidated sands with plastic fines in a void ratio range of 0.4 – 1.0. Sand matrices with a uniformity in a range of 1.68 – 2.76 were tested; thus, the proposed coefficients should be considered with care if different sand matrices are going to be predicted.

Acknowledgement

This article was created with the support of the Ministry of Education, Science, Research and Sport of the Slovak Republic within VEGA Grant No. 1/0842/18.

REFERENCES

Atkinson, J., Sallfors, G., (1991) *Experimental determination of soil properties*. Proceedings of 10th ECSMFE, Florence, Vol. 3, pp. 915-956.

Benz, T., (2007) *Small Strain Stiffness of Soils and Its Numerical Consequences*. Mitteilung 55 des Instituts fur Geotechnik der Universitat of Stuttgart, p. 187.

Carraro, J., Prezzi, M., Salgado, R., (2009) S*hear Strength and Stiffness of Sands Containing Plastic or Nonplastic Fines*. Journal of Geotechnical and Geoenvironmental Engineering, 135(9), pp. 1167-1178.

Goudrazy, M., Rahman, M., Konig, D., Schanz, T., (2016) *Influence of Non-Plastic Fines Content on Maximum Shear Modulus of Granular Materials*. Soils and Foundations, 56(6), pp. 973-983.

Greening, P., Nash, D., (2004) *Frequency domain determination of G0 using bender elements*. Geotechnical Testing Journal, 27(3), pp. 1-7.

Gu, X., Yang, J., Huang, M., (2013) *Laboratory Measurements of Small Strain Properties of Dry Sands by Bender Element*. Soils and Foundations, 53(5), pp. 735-745.

Gu, X., Yang, J., Huang, M., Gao, G., (2015) *Bender Element Tests in Dry and Saturated Sand: Signal Interpretation and Result Comparison*. Soils and Foundations, 55(5), pp. 952-963.

Hardin, B., Drnevich, V., (1972) *Shear Modulus and Damping in Soils: Design Equations and Curves*. Journal of the Soil Mechanics and Foundations Division, ASCE(SM7), pp. 667-692.

Hardin, B., Richart, F., (1963) *Elastic wave velocities in granular soils*. Journal of Soil Mechanics and Foundations Division, 89(SM 1), pp. 33-65.

Ishibashi, I., Zhang, X., (1993) *Unified Dynamic Shear Moduli and Damping Ratios of Sand and Clay*. Soils and Foundations, 33(1), pp. 182-191.

Iwasaki, T., Tatsuoka, F., (1977) *Effects of grain size and grading on dynamics shear moduli of sands*. Soils and Foundations, 17(3), pp. 19-35.

Jamiolkowski, M., Leroueil, S., Lo Presti, D., (1991) *Theme lecture: Design Parameters from Theory to Practice*. Proceedings of Geo-Coast, pp. 1-41.

Jovicic, V., Coop, M., Simic, M., (1996) *Objective criteria for determining Gmax from bender element tests*. Géotechnique, 46(2), pp. 357-362.

Lee, J., Santamarina, C., (2005) *Bender Elements: Performance and Signal Interpretation*. Journal of Geotechnical and Geoenvironmental Engineering, 131(9), pp. 1063-1070.

Lings, M., Greening, P., (2001) *A novel bender/extender element for soil testing*. Géotechnique, 51(8), pp. 713-717.

Lo Presti, D. et al., (1993) *Monotonic and Cyclic Loading Behaviour of Two Sands*. Geotechnical Testing Journal, 16(4), pp. 409-424.

MathWorks Inc., (2017a) *MatLab*. Natick, Mass., USA.

Ogino, K., Kawaguchi, T., Yamashita, S., Kawajiri, S., (2015) *Measurement deviations for shear wave velocity of bender ele-*

ment test using time domain, cross-correlation, and frequency domain approaches. Soils and Foundations, 55(2), pp. 329-342.

Oztoprak, S., Bolton, M., (2013) *Stiffness of Sands Through a Laboratory Test Database*. Géotechnique, 63(1), pp. 54-70.

Panuška, J., (2018) *Elastic properties of natural sands with fines measured by bender / extender elements*. Dissertation thesis, Dept. of Geotechnics, Slovak University of Technology, p. 233.

Payan, M., Khoshghalb, A., Senetakis, K., Khalili, N., (2016a) *Effect of Particle Shape and Validity of Gmax Models for Sand: A Critical Review and a New Expression*. Computers and Geotechnics, Vol. 72, pp. 28-41.

Paydar, N., Ahmadi, M., (2016) *Effect of Fines Type and Content of Sand on Correlation Between Shear Wave Velocity and Liquefaction Resistance*. Geotechnical and Geological Engineering, 34(6), pp. 1857-1876.

Rohatgi, A., (2017) WebPlotDigitizer. https://automeris.io/WebPlotDigitizer.

Salgado, R., Bandini, P. & Karim, A., (2000) *Shear Strength and Stiffness of Silty Sand*. Journal of Geotechnical and Geoenvironmental Engineering, 126(5), pp. 451-462.

Sanchez-Salinero, I., Roesset, J., Stokoe, K., (1986) *Analytical studies of body wave propagation and attenuation*. Geotechnical Engineering Center, Civil Engineering Department, Univ. of Texas at Austin, Report GR86-15, p. 272.

Senetakis, K., Anastasiadis, A., Pitilakis, K., (2012) *The Small Strain Shear Modulus and Damping Ratio of Quartz and Volcanic Sands.* Geotechnical Testing Journal, 35(6), pp. 1-17.

Senetakis, K. et al., (2017) *Experimental Investigation of Primary-Wave Velocities and Constrained Moduli of Quartz Sand Subjected to Extender Element Tests and Stress Anisotropy*. Geomechanics and Geophysics for Geo-Energy and Geo-Resources, 3(2), pp. 211-219.

Shibuya, S., Hwang, S., Mitachi, T., (1997) *Elastic Shear Modulus of Soft Clays from Shear Wave Velocity Measurement*. Géotechnique, 47(3), pp. 593-601.

Shirley, D., Hampton, L., (1978) *Shear-wave measurements in laboratory sediments*. The Journal of the Acoustical Society of America, 63(2), pp. 607-613.

Schultheiss, P., (1981) *Simultanous Measurement of P and S Wave Velocities During Conventional Laboratory Soil Testing Procedures*. Marine Geotechnology, 4(4), pp. 343-367.

Szilvágyi, Z., (2018) *Dynamic Soil Properties of Danube Sands*. Dissertation thesis, Department of Structural and Geotechnical Engineering, Széchenyi István University Győr, p. 127.

Viana Da Fonseca, A., Ferreira, C., Fahey, M., (2008) *A framework interpreting bender element tests, combining time-domain and frequency-domain methods*. Geotechnical Testing Journal, 32(2), pp. 1-17.

Wichtmann, T., Navarrete Hernández, M., Triantafyllidis, T., (2015) *On the Influence of Non-Cohesive Fines Content on Small Strain Stiffness, Modulus Degradation and Damping of Quartz Sand*. Soil Dynamics and Earthquake Engineering, Volume 69, pp. 103-114.

Wichtmann, T., Triantafyllidis, T., (2009) *Influence of the Grain-Size Distribution Curve of Quartz Sand on the Small Strain Shear Modulus Gmax*. Journal of Geotechnical and Geoenvironmental Engineering, Vol. 135, pp. 1404-1418.

Wichtmann, T., Triantafyllidis, T., (2010) *On the Influence of the Grain Size Distribution Curve on P - Wave Velocity and Constrained Elastic Modulus Mmax and Poisson´s Ratio of Quartz Sand*. Soil Dynamics and Earthquake Engineering, Vol. 30, pp. 757-766.

Yamashita, S. et al., (2009) *Interpretation of international parallel test on the measurement of Gmax using bender elements*. Soils and Foundation, 49(4), pp. 631-650.

Yang, J., Liu, X., (2016) *Shear Wave Velocity and Stiffness of Sand: The Role of Non-Plastic Fines*. Géotechnique, 66(6), pp. 500-514.